




Unveiling the role of UPF3B in hepatocellular carcinoma: Potential therapeutic target

Bowen Hou¹ | Min Shu¹  | Chenghao Liu¹  | Yunfeng Du¹ | Cuicui Xu¹ |
Huijiao Jiang^{1,2} | Jun Hou^{1,2} | Xueling Chen^{1,2} | Lianghai Wang^{1,2}  | Xiangwei Wu^{1,2}

¹NHC Key Laboratory of Prevention and Treatment of Central Asia High Incidence Diseases, The First Affiliated Hospital/Shihezi University School of Medicine, Shihezi, China

²Key Laboratory of Xinjiang Endemic and Ethnic Diseases, Shihezi University School of Medicine, Shihezi, China

Correspondence

Lianghai Wang and Xiangwei Wu, NHC Key Laboratory of Prevention and Treatment of Central Asia High Incidence Diseases, The First Affiliated Hospital/Shihezi University School of Medicine, North 2nd Road, Shihezi 832000, Xinjiang, China.

Email: lh_wang@shzu.edu.cn and wxxshz@126.com

Funding information

Non-profit Central Research Institute Fund of Chinese Academy of Medical Sciences, Grant/Award Number: 2020-PT330-003; National Natural Science Foundation of China, Grant/Award Number: 82360503; Bingtuan Science and Technology Program, Grant/Award Number: 2021BC002; Tianshan Talents - Science and Technology Innovation Team Project, Grant/Award Number: 2023TSYCTD0020

Abstract

RNA-binding proteins can regulate nucleotide metabolism and gene expression. UPF3B regulator of nonsense mediated mRNA decay (UPF3B) exhibits dysfunction in cancers. However, its role in the progression of hepatocellular carcinoma (HCC) is still insufficiently understood. Here, we found that UPF3B was markedly upregulated in HCC samples and associated with adverse prognosis in patients. UPF3B dramatically promoted HCC growth both in vivo and in vitro. Mechanistically, UPF3B was found to bind to *PPP2R2C*, a regulatory subunit of PP2A, boosting its mRNA degradation and activating the PI3K/AKT/mTOR pathway. E2F transcription factor 6 (E2F6) directly binds to the UPF3B promoter to facilitate its transcription. Together, the E2F6/UPF3B/PPP2R2C axis promotes HCC growth through the PI3K/AKT/mTOR pathway. Hence, it could be a promising therapeutic target for treating HCC.

KEYWORDS

E2F6, HCC, PI3K/AKT/mTOR pathway, PPP2R2C, UPF3B

Abbreviations: CNV, copy number variation; E2F6, E2F transcription factor 6; HCC, hepatocellular carcinoma; KEGG, Kyoto Encyclopedia of Genes and Genomes; METTL, methyltransferase-like; NMD, nonsense-mediated mRNA decay; PP2A, protein phosphatase 2A; PPP2R2C, protein phosphatase 2 regulatory subunit Bgamma; qRT-PCR, quantitative RT-PCR; RBP, RNA-binding protein; RIP, RNA immunoprecipitation; RIP-seq, RIP sequencing; RNA-seq, RNA sequencing; TCGA, The Cancer Genome Atlas; UPF3B, UPF3B regulator of nonsense mediated mRNA decay.

Bowen Hou and Min Shu contributed equally to this work.

This is an open access article under the terms of the [Creative Commons Attribution-NonCommercial](https://creativecommons.org/licenses/by-nc/4.0/) License, which permits use, distribution and reproduction in any medium, provided the original work is properly cited and is not used for commercial purposes.

© 2024 The Author(s). *Cancer Science* published by John Wiley & Sons Australia, Ltd on behalf of Japanese Cancer Association.

1 | INTRODUCTION

Global Cancer Statistics 2022 highlights that primary liver cancer holds the sixth position in terms of incidence and is ranked third in mortality among all malignant tumors.¹ Liver cancer is a common primary tumor, with HCC accounting for 75%–85% of the diagnoses. Despite a decline in mortality for many cancers, HCC remains one of the fastest-growing causes of cancer-linked fatalities worldwide.^{1,2} As a significant histologic subtype of liver cancer, HCC is characterized by a high risk of recurrence and heterogeneity, and there are currently few alternatives available for targeted therapy.^{3–5} Therefore, discovering novel molecular targets that impact the onset and progression of HCC is crucial for both clinical diagnosis and the development of treatment approaches.

RNA binding proteins are a broad class of proteins that interact with transcript and noncoding RNAs. They bind to RNAs through one or more of their RNA-binding domains, regulating nucleotide metabolism of the bound RNAs and gene expression.^{6,7} Approximately 1500 RBPs have been validated experimentally in humans, accounting for approximately 7% of all coding genes.⁸ Numerous human diseases, including cancer and neurological disorders, could be caused by RBP dysfunction.^{9,10} UPF3B is a core junction protein in the NMD pathway, involved in the exonuclear transport and quality supervision of mRNA, based on identifiable NMD-inducing features such as the exon-junction complex and long 3'-UTRs.^{11,12} Nonsense-mediated mRNA decay is a highly protective RNA degradation mechanism that detects and represses aberrant mRNAs carrying premature termination codons, thus ensuring correct gene expression.¹³ Mammalian UPF3B is found to activate NMD without binding to the exon junction complex.¹⁴ UPF3B shows promise as a genetic prognostic modeling factor for predicting the progression of diverse tumor types, such as esophageal cancer, chromophobe renal cell carcinoma, and cutaneous melanoma.^{15,16} Despite these findings, the role of UPF3B in HCC still needs to be explored.

This study found that UPF3B showed heightened expression in HCC tissues and was linked with adverse prognosis. Furthermore, the acquired data indicated the involvement of PPP2R2C in the UPF3B-mediated activation of the PI3K/AKT/mTOR pathway. The study also noted that E2F6 could bind to UPF3B promoters to up-regulate UPF3B expression and promote the development of HCC. The data acquired in this research highlight the potential of UPF3B to function as a therapeutic target.

2 | MATERIALS AND METHODS

2.1 | Bioinformatic analysis

The evaluation of UPF3B expression in pan-cancer involved utilizing data from 33 tumor types sourced from TCGA data. Clinical data of 374 HCC tissue samples and 50 samples of normal liver tissues contained in the TCGA-LIHC cohort was accessed at the Genomic Data Commons (<https://portal.gdc.cancer.gov/>). The

RNA-seq data were downloaded, preprocessed by R software (R Foundation for Statistical Computing), and integrated with the corresponding clinical data. The Wilcoxon rank sum test was adopted to compare gene expression levels in tumor and normal tissues. Correlations between gene expression and several clinical variables were analyzed using univariate and multivariate Cox regression analysis. Survival analysis was undertaken using the Survival package of R software to explore the effect of the selected genes on overall (using the median value as a cut-off), disease-free, disease-specific, and progression-free survival (using the optimal cut-off with a minimal *p* value).

Expression profiling of 225 hepatitis B virus-related HCC samples was retrieved from the GSE14520 dataset (GPL3921 platform) in the Gene Expression Omnibus repository and preprocessed by R software. Correlations between gene expression were analyzed using Spearman's correlation analysis. Survival analysis was carried out using the Survival package of R software to explore the effect of the selected genes on overall survival using the optimal cut-off with a minimal *p* value.

2.2 | Gene Set Enrichment Analysis

The RNA-seq expression matrix of TCGA-LIHC was used to identify signaling pathways associated with UPF3B expression levels by Gene Set Enrichment Analysis (version 4.1.0; UC San Diego/Broad Institute) software. A false discovery rate of less than 0.05 was considered statistically significant.

2.3 | Cell culture

Human HCC cell lines, including HepG2, Hep3B, HuH-7, and SNU-387, were obtained from the National Collection of Authenticated Cell Cultures. The human HCC cell lines of MHCC97H were obtained from Beyotime Biotech. Cells were cultured in DMEM or RPMI-1640 medium (Gibco), supplemented with 10% FBS (Gibco) and 1% penicillin-streptomycin solution (Beijing Solarbio Science & Technology) in an incubator at 37°C under 5% CO₂.

2.4 | Cell transfection

The UPF3B overexpression plasmid and control pEX-4 plasmid (Shanghai GenePharma) were introduced into cells showing low expression of UPF3B utilizing Lipofectamine 2000 (Invitrogen) per the manufacturer's instructions. Cells with stable high expression of UPF3B were obtained after being screened using kanamycin. siRNA and scramble control (GenePharma) were introduced into cells using Lipofectamine RNAiMAX (Invitrogen). siRNA oligonucleotide sequences are listed in Table S1. UPF3B-interfering lentiviruses (GenePharma) were delivered into cells with high expression of UPF3B per the manufacturer's instructions, and cells were

further screened using a 1.25 µg/mL puromycin to obtain stable UPF3B-silenced cells. The E2F6 overexpression plasmid and control pcDNA3.1(+) vector (GenePharma) were introduced into MHCC97H and HepG2 cells with Lipofectamine 3000 (Invitrogen) per the given instructions. Cells with stable E2F6 overexpression were obtained after screening using G418.

2.5 | Quantitative RT-PCR

The extraction of total RNA from cultured cells or tissues involved using E.N.Z.A. Total RNA Kit I (R6834-01, OMEGA). After reverse transcription of the isolated RNA into cDNA using the RevertAid First Stand cDNA Synthesis Kit (Thermo Fisher Scientific), qRT-PCR was carried out. This analysis was executed utilizing the FastSYBR Mixture provided by Beijing CoWin Biotech in a CFX96 Touch Real-Time PCR Detection System (Bio-Rad Laboratories). β -Actin was set as the reference gene. The primers used for this analysis were obtained from GenePharma, see [Table S1](#).

2.6 | Western blot analysis

Total cellular proteins were extracted by utilizing the RIPA Lysis Buffer from Sigma-Aldrich. Protein concentration was quantified using the BCA Kit for Protein Determination (Thermo Fisher Scientific). The extracted protein solution was electrophoresed by SDS-PAGE and transferred to a 0.22 µm PVDF membrane (Millipore Corporation). After blocking using 5% BSA (Solarbio), the membranes were exposed to Abs against UPF3B (1:2000, ab134566; Abcam), p-AKT (1:2000, #4060; Cell Signaling Technology), AKT (1:2000, #4691; Cell Signaling Technology), p-S6 (1:2000, #4858; Cell Signaling Technology), S6 (1:2000, #2217; Cell Signaling Technology), E2F6 (1:10000, ab155978; Abcam), and GAPDH (1:10000, TA-08; ZSGB-Bio) overnight at 4°C. Subsequently, the membrane was washed and incubated with secondary Abs for 1 h at room temperature. Protein bands were detected using an enhanced chemiluminescence reagent (Millipore). The signal intensity was quantified to calculate relative levels of UPF3B and E2F6 normalized with GAPDH, p-AKT normalized with total AKT, and p-S6 normalized with total S6.

2.7 | CCK-8 assay

The cell proliferation assay was undertaken using CCK-8 provided by Dojindo Laboratories. Cells were seeded in 96-well plates at a density of 2000 cells per well and kept at 37°C for 0, 24, 48, and 72 h in an incubator under 5% CO₂. After the incubation period, 10 µL CCK-8 reagent was introduced to each well, and the cells were incubated at 37°C for another 2 h, protected from light. A Multiskan FC Microplate Photometer (Thermo Fisher Scientific) was utilized to quantify the absorbance at 450 nm.

2.8 | Colony formation assay

Cells were inoculated in 6-well plates at a density of 2000 cells per well. After 2–3 weeks of culture, the cells were fixed with 4% paraformaldehyde (Solarbio) for 30 min and then exposed to 1% Crystal Violet-Gentian Violet Stain Solution (Solarbio) for another 30 min. Photographs were taken, and colonies with more than 50 cells were counted using ImageJ software (NIH).

2.9 | EdU staining

Cells were spread in 12-well plates and kept at 37°C for 24 h. The next day, fixation and staining were carried out using EdU Imaging Kits (cy3) provided by APEX BIO Technology per the given protocol. The cells were observed and photographed under a microscope.

2.10 | RNA-seq

Total RNA was extracted from shCtrl- and shUPF3B-treated MHCC97H cells using TRIzol reagent (Invitrogen). The quantity and purity of total RNA were analyzed using Bioanalyzer 2100 and RNA 6000 Nano LabChip Kit (Agilent). After purification, the mRNA was fragmented using divalent cations under elevated temperatures. The cleaved RNA fragments were then reverse-transcribed to cDNA using the SuperScript II Reverse Transcriptase (Invitrogen). Next, U-labeled second-stranded DNAs were synthesized by *Escherichia coli* DNA polymerase I (NEB), RNase H (NEB), and dUTP Solution (Thermo Fisher Scientific). An A-base was then added to the blunt ends of each strand. After the heat-labile UDG enzyme (NEB) treatment of the U-labeled second-stranded DNAs, the ligated products were amplified with PCR. Finally, paired-end sequencing was carried out on an Illumina Novaseq 6000 by Hangzhou Lianchuan Biotechnology.

2.11 | RNA immunoprecipitation sequencing

Lysates of shCtrl- and shUPF3B-treated MHCC97H cells were incubated with UPF3B Ab (ab134566; Abcam) or isotype control IgG. The RNA-protein complexes were immunoprecipitated with protein A/G magnetic beads. The beads were then washed with ice-cold NT2 buffer five times. TRIzol reagent (Invitrogen) was used to isolate total RNA. Sample libraries were prepared with SMART-Seq version 4 Ultra Low Input RNA Kit for Sequencing (Takara Bio). Libraries were sequenced on an Illumina NovaSeq 6000 by Hangzhou Lianchuan Biotechnology.

2.12 | RNA stability assay

After 24 h of cell transfection, actinomycin D (MedChemExpress) at a final concentration of 10 µg/mL was introduced to the culture

medium and incubated until the indicated time. Quantitative RT-PCR analysis was carried out to determine the *PPP2R2C* mRNA levels in the actinomycin D-treated group at different time points.

2.13 | Screening of transcription factors related to UPF3B

The database hTFtarget (<https://bioinfo.life.hust.edu.cn/hTFtarget>) was utilized to screen transcription factors associated with *UPF3B* promoter, cBioPortal (<http://cbioportal.org>) was used to screen for genes correlated with *UPF3B* with a correlation coefficient >0.3. The binding scores of transcription factors on *UPF3B* were evaluated by Cistrome Data Browser (<http://cistrome.org/db>), and JASPAR (<https://jaspar.genereg.net>) was utilized to predict the relevant binding sites on *UPF3B* promoter.

2.14 | Chromatin immunoprecipitation

Chromatin immunoprecipitation assay was undertaken using the SimpleChIP Enzymatic Chromatin IP Kit (Agarose Beads) (#9002; Cell Signaling Technology). Briefly, HepG2 cells were fixed with formaldehyde, and cross-linked chromatin was enzymatic fragmented. Protein A/G beads were pretreated before incubation with anti-E2F6 Ab. Immunoglobulin G served as a negative control in the experiments. After cross-link reversal, qRT-PCR was utilized to assess the binding of E2F6 to the promoter of *UPF3B*.

2.15 | Mouse xenograft models

BALB/C nude mice aged 4–5 weeks were purchased from SPF (Beijing) Biotechnology and randomly grouped. MHCC97H cells in the logarithmic growth phase were suspended in a 1:1 mixture, containing 3×10^6 cells/mouse and Matrigel, and then s.c. injected into the mice. The size of the tumor was measured every 3 days. Tumor volume was calculated by the formula $(\text{length}^2 \times \text{width})/2$. At the end of the experiment, mice were killed, tumors were excised and weighed, and tissue proteins were extracted using the Tissue or Cell Total Protein Extraction Kit (C510003; Sangon Biotech). The experimental protocols utilized in this research were approved by the Biology Ethics Committee of Shihezi University.

2.16 | Human HCC samples

Primary tumor tissues and corresponding paracancerous tissues were acquired from patients with HCC at the First Affiliated Hospital of Shihezi University with informed consent. The proteins were extracted by the FFPE Total Protein Extraction Kit (C500058; Sangon). The study protocol was approved by the Science and

Technology Ethical Committee of the First Affiliated Hospital of Shihezi University.

2.17 | Statistical analysis

Data are expressed as mean \pm SD. Statistical significance was analyzed using GraphPad Prism 8.0 (GraphPad Software). The variance across the experimental and control groups was comparatively assessed by unpaired *t*-test or ANOVA. The differences in the survival rate of HCC patients were compared using the Kaplan–Meier curve and log-rank test. $p < 0.05$ indicates that the difference is statistically significant.

3 | RESULTS

3.1 | UPF3B highly expressed in HCC and linked to poor prognosis

According to the RNA-seq data from the TCGA database, *UPF3B* transcript showed significantly higher levels in various tumors, including HCC, compared to the corresponding normal tissues (Figure 1A,B). On further examination of the clinical data of individuals with HCC, elevated *UPF3B* expression was observed in patients with advanced histologic grades and pathologic stages (Figure 1C). Univariate and multivariate Cox regression analysis of clinical parameter variables, including patient age, gender, tumor grade, and stage, indicated that *UPF3B* expression could be used as an independent predictive factor for predicting the overall survival of the patient (Figure 1D). The Kaplan–Meier survival analysis showed that patients with high *UPF3B* expression had decreased overall, disease-free, disease-specific, and progression-free survival (Figure 1E). These results reveal that high *UPF3B* expression is linked to poor prognosis in individuals with HCC.

3.2 | UPF3B promotes HCC cell proliferation

To investigate the potential role of *UPF3B* in HCC, tumor samples from TCGA-LIHC were grouped into high and low *UPF3B* expression using the median value as a cut-off. Subsequently, KEGG pathway enrichment analysis was carried out. As shown in Figure 2A, the cell cycle pathway is one of the top enriched pathways in the *UPF3B*-high group. Therefore, it was inferred that the high expression of *UPF3B* could promote the proliferation of HCC cells. To verify the above inference, *UPF3B* expression was initially examined in a panel of HCC cell lines (Figure 2B). Subsequently, HepG2 and MHCC97H cells with high *UPF3B* expression were selected for *UPF3B* interference. Quantitative RT-PCR and western blot analysis were carried out to verify the efficiency of *UPF3B* knockdown in HepG2 and MHCC97H cells (Figure 2C,D). The CCK-8 assay (Figure 2E), colony formation assay (Figure 2F), and EdU assay (Figure 2G,H) showed attenuated

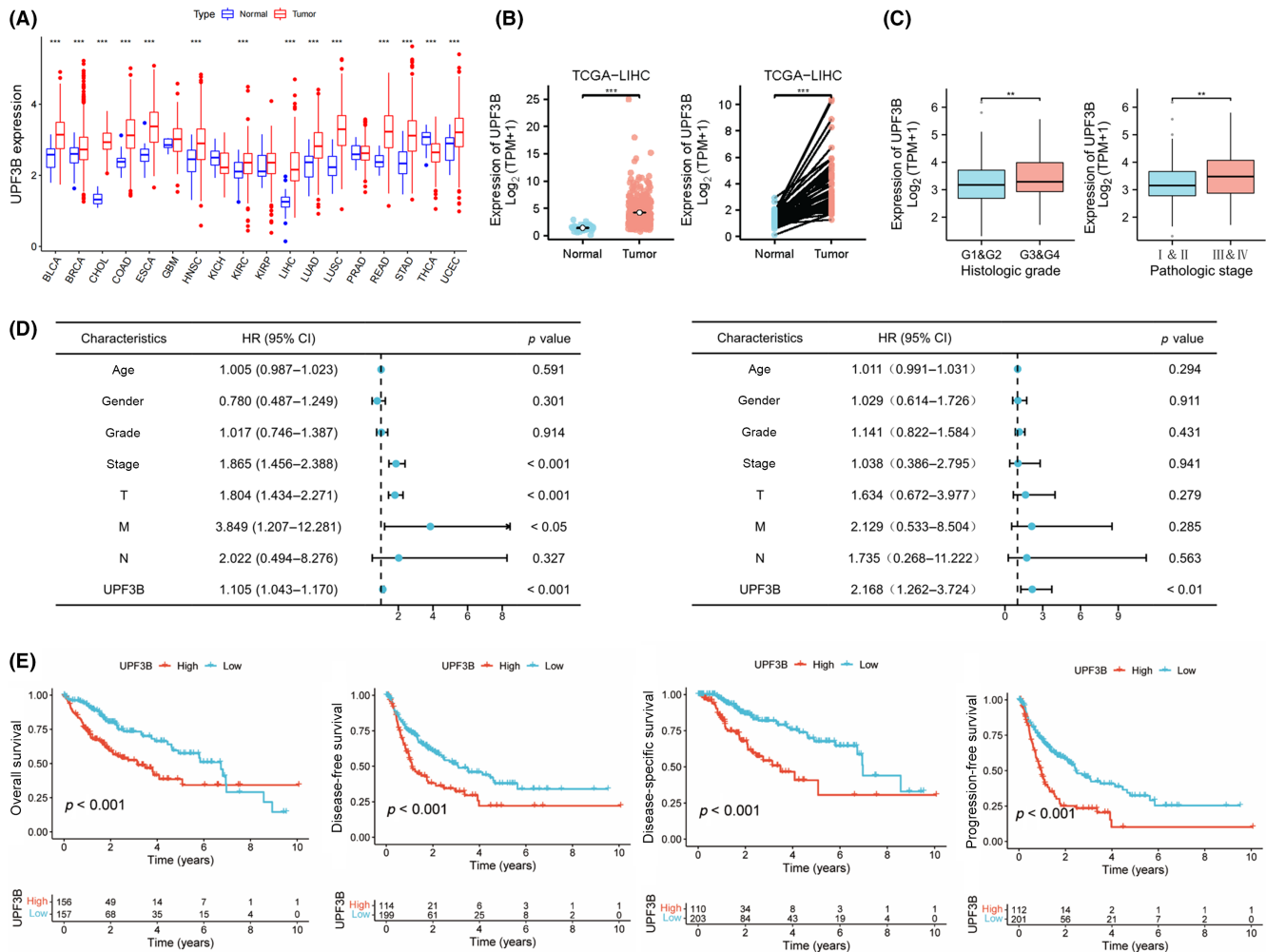


FIGURE 1 *UPF3B* is upregulated and correlates with poor survival noted in patients with hepatocellular carcinoma (HCC). (A) Expression of *UPF3B* in different types of tumor samples and normal tissues in The Cancer Genome Atlas (TCGA). (B) *UPF3B* mRNA levels in the TCGA-LIHC dataset. (C) *UPF3B* expression in patients with the indicated histologic grades and pathologic stages. (D) Univariate and multivariate Cox regression analyses of the association between *UPF3B* expression and clinicopathologic characteristics. (E) Kaplan–Meier analysis of the association between *UPF3B* expression and overall, disease-free, disease-specific, and progression-free survival in patients with HCC. ** $p < 0.01$, *** $p < 0.001$. CI, confidence interval; HR, hazard ratio.

growth, decreased colony numbers, and reduced proportion of EdU⁺ cells, indicating that knocking down *UPF3B* considerably suppressed the proliferation of HepG2 and MHCC97H cells compared with the control group. In vivo experiments also highlighted that the knockdown of *UPF3B* inhibited s.c. tumor growth (Figure 2I–K).

In contrast, after ectopic upregulation of *UPF3B* transcript and protein levels in Hep3B, SNU-387, and HuH-7 cells with endogenous low *UPF3B* expression (Figure S1A,B), CCK-8, colony formation, and EdU assays showed that overexpression of *UPF3B* significantly promotes the proliferation of these cells (Figure S1C–E).

3.3 | *UPF3B* activates PI3K/AKT/mTOR signaling

To explore the underlying mechanism of *UPF3B* in facilitating the proliferation of HCC cells, an enrichment analysis of the Hallmark

gene sets was undertaken on TCGA-LIHC grouped according to different expression levels of *UPF3B*. As shown in Figure 3A, mTORC1 signaling and PI3K/AKT/mTOR signaling were the top enriched pathways in the *UPF3B* high-expression group. After the overexpression of *UPF3B* in Hep3B, SNU-387, and HuH-7 cells, western blotting indicated that phosphorylation levels of the critical proteins AKT and S6 in the PI3K/AKT/mTOR pathway were elevated (Figure 3B). In contrast, the knockdown of *UPF3B* in HepG2 and MHCC97H cells resulted in decreased levels of p-AKT and p-S6 (Figure 3C). Subsequently, three cell lines showing low *UPF3B* expression were chosen for *UPF3B* overexpression and treatment with rapamycin (mTORC1 inhibitor) and MK2206 (AKT inhibitor) (Figure 3D). CCK-8, EdU, and colony formation assays showed that the promotion of cell proliferation by *UPF3B* could be reversed by AKT and mTORC1 inhibitor treatments in SNU-387, Hep3B, and HuH-7 cells (Figures 3E,F and S2).

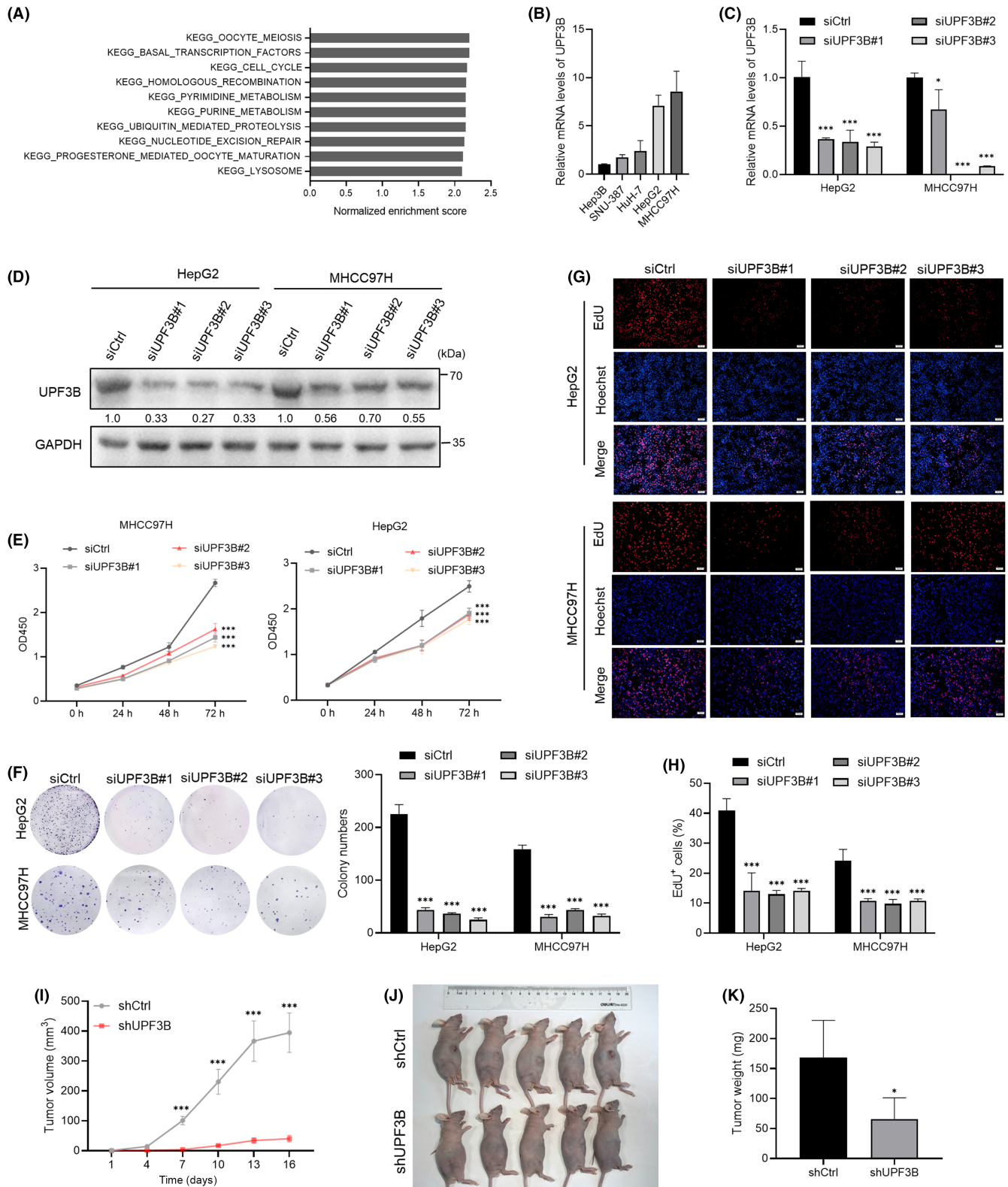


FIGURE 2 Knockdown of UPF3B inhibits hepatocellular carcinoma (HCC) growth. (A) Top 10 enriched Kyoto Encyclopedia of Genes and Genomes (KEGG) pathways in tumors with high UPF3B from The Cancer Genome Atlas (TCGA)-LIHC dataset by Gene Set Enrichment Analysis. (B) Expression of *UPF3B* in HCC cell lines. (C) Expression of UPF3B was examined by quantitative RT-PCR in control and UPF3B-knocked down cells. (D) Protein levels of UPF3B were determined by western blotting in control and UPF3B-knocked down cells. (E) CCK-8 assay for HCC cells with UPF3B knockdown. (F) Colony formation assays for HCC cells with UPF3B knockdown. (G) Representative images and (H) statistical analysis of EdU⁺ cells after UPF3B knockdown. (I) Subcutaneous xenograft volume was measured every 3 days. (J) Images and (K) weight of tumors collected at 16 days postinoculation ($n = 5$). * $p < 0.05$, *** $p < 0.001$. OD450, optical density at 450 nm.

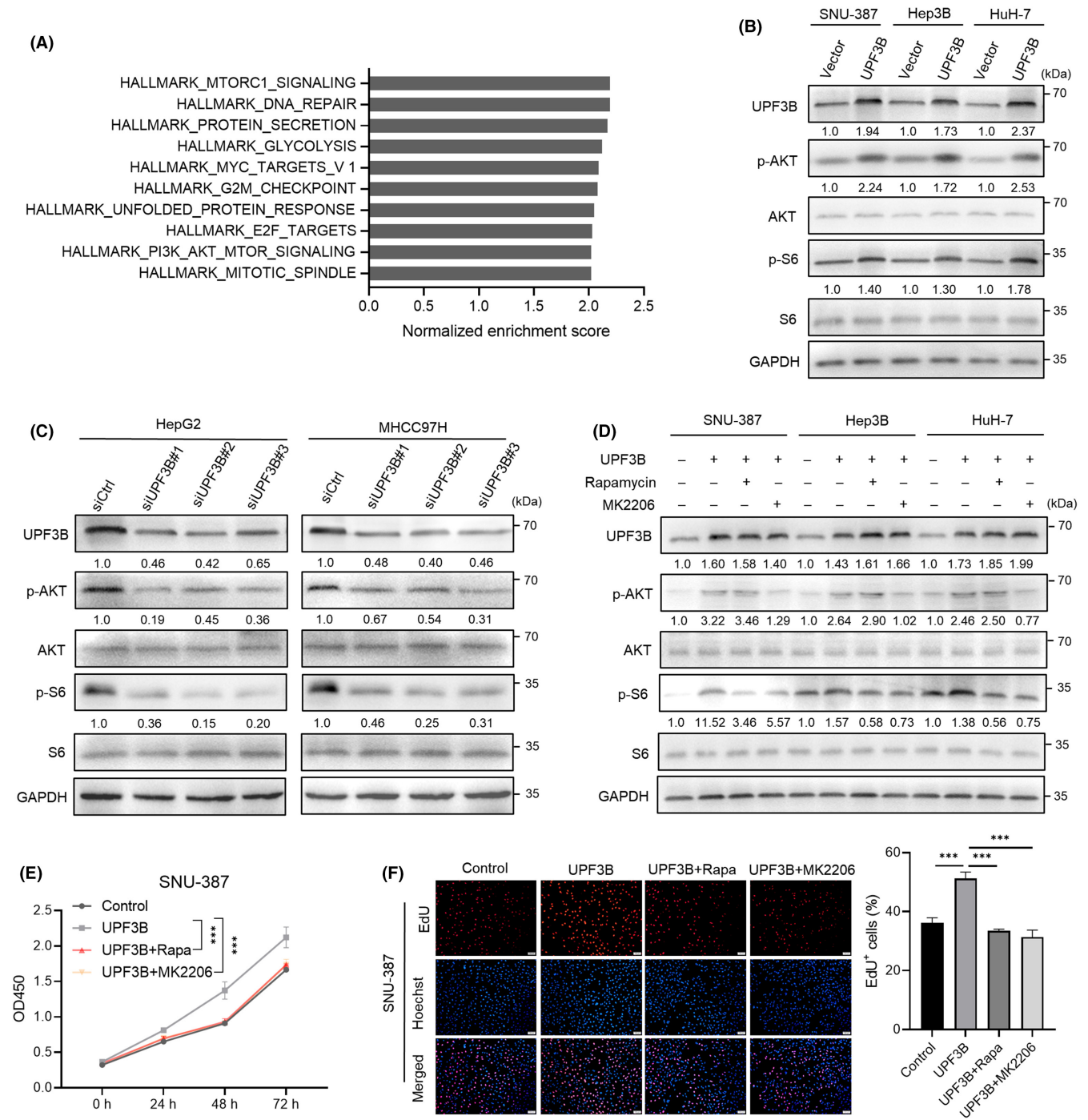


FIGURE 3 UPF3B promotes the activation of PI3K/AKT/mTOR signaling. (A) Top 10 enriched HALLMARK gene sets in tumors with high UPF3B from The Cancer Genome Atlas (TCGA)-LIHC dataset by GSEA. Western blotting of proteins associated with the PI3K/AKT/mTOR signaling pathway following the (B) overexpression or (C) knockdown of UPF3B. (D) Western blotting of proteins associated with the PI3K/AKT/mTOR signaling pathway after AKT and mTORC1 inhibitors treatment. (E) CCK-8 and (F) EdU assays for SNU-387 cells following UPF3B overexpression and treatment with mTORC1 inhibitor and AKT inhibitor. *** $p < 0.001$. OD450, optical density at 450 nm.

3.4 | PPP2R2C implicated in UPF3B-mediated activation of PI3K/AKT/mTOR pathway

Given that UPF3B can bind and degrade specific target mRNAs,^{11,12} RNA-seq and RIP-seq were carried out on control and UPF3B knockdown MHCC97H cells to identify UPF3B target genes. Genes that

were upregulated in RNA-seq ($\log_2FC \geq 1$ and $q < 0.05$) and with decreased binding in RIP-seq ($\log_2FC \leq -1$ and p value < 0.05) upon UPF3B interfering can be considered UPF3B-dependent NMD targets. The KEGG enrichment analysis showed that 26 genes were enriched in the PI3K/AKT pathway (Figure 4A, Table S2), including upstream suppressors such as PPP2R2C, a regulatory subunit of

the serine/threonine-specific phosphatase (PPP2R2A). Previous studies have shown that PPP2R2C can participate in the aging process by inhibiting the phosphorylation of mTOR and AKT.¹⁷ Quantitative

RT-PCR analysis confirmed that the expression levels of PPP2R2C were elevated after interfering with UPF3B in HepG2 and MHCC97H cells (Figure 4B). In contrast, the levels of PPP2R2C were decreased

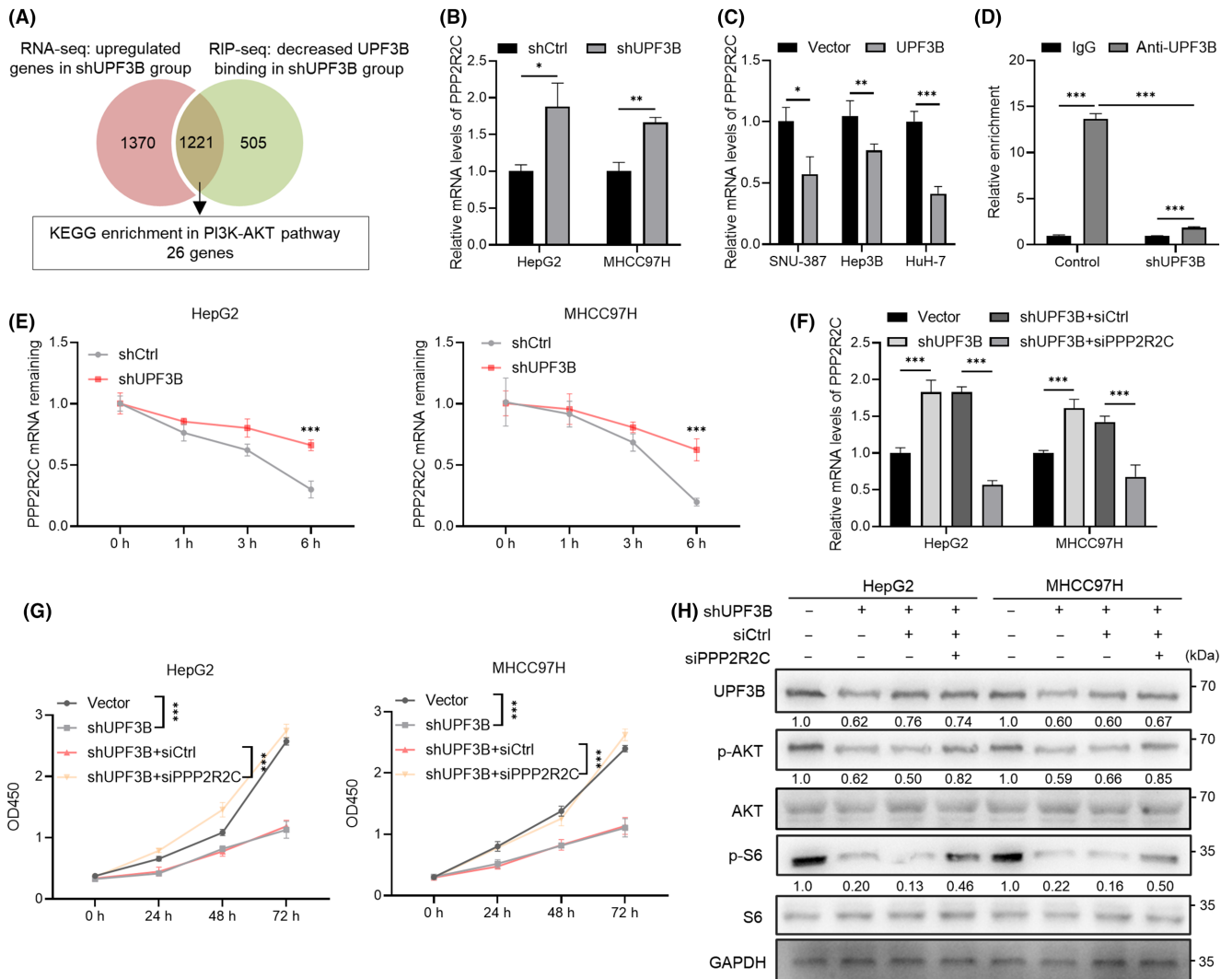
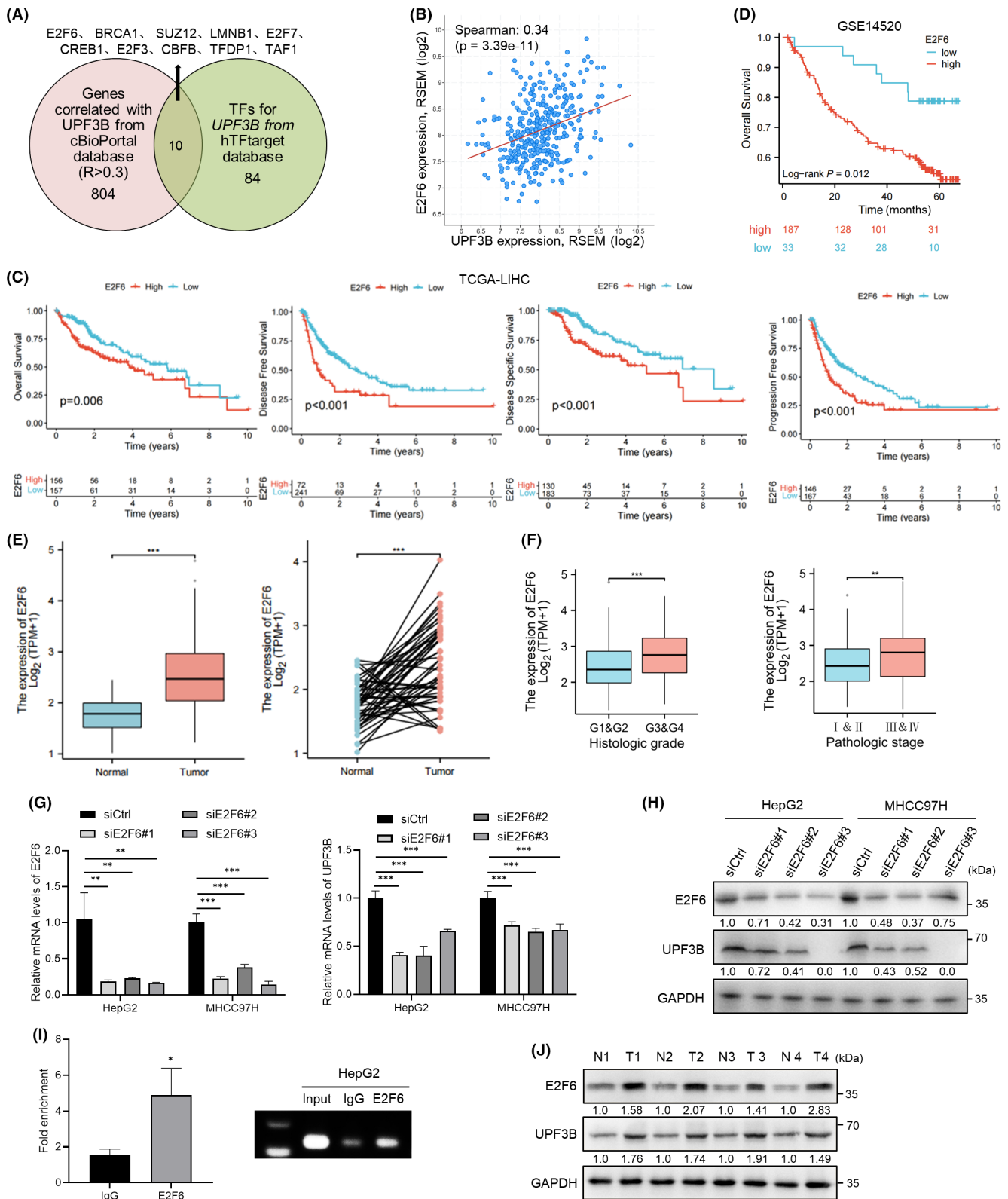


FIGURE 4 PPP2R2C is involved in UPF3B-mediated PI3K/AKT/mTOR signaling activation. (A) Screening of UPF3B target genes by combining RNA sequencing (RNA-seq), RNA immunoprecipitation sequencing (RIP-seq), and Kyoto Encyclopedia of Genes and Genomes (KEGG) enrichment analyses. Expression of PPP2R2C in (B) UPF3B knocked down and (C) UPF3B overexpressed hepatocellular carcinoma (HCC) cells was detected by quantitative RT-PCR (qRT-PCR). (D) Binding of UPF3B with PPP2R2C mRNA was confirmed by RIP and qRT-PCR in MHCC97H cells. (E) PPP2R2C mRNA levels in control and UPF3B knocked down HCC cells after treatment with 10 μg/mL actinomycin D for the indicated time points. (F) PPP2R2C mRNA expression in HCC cells treated with shUPF3B and siPPP2R2C was examined by qRT-PCR. (G) CCK-8 assay for HCC cells treated with shUPF3B and siPPP2R2C. (H) Western blotting of proteins associated with the PI3K/AKT/mTOR signaling after shUPF3B and siPPP2R2C treatment. **p* < 0.05, ***p* < 0.01, ****p* < 0.001. OD450, optical density at 450 nm.

FIGURE 5 E2F6 promotes UPF3B transcription. (A) Screening of potential UPF3B transcription factors (TFs) using hTFtarget and cBioPortal databases. (B) Correlation between E2F6 and UPF3B expression levels in The Cancer Genome Atlas (TCGA)-LIHC dataset. (C) Kaplan–Meier analysis of the association between E2F6 expression and overall, disease-free, disease-specific, and progression-free survival in TCGA-LIHC dataset. (D) Kaplan–Meier analysis of the association between E2F6 expression and overall survival in the GSE14520 dataset. (E) E2F6 mRNA levels in normal and tumor samples from TCGA-LIHC dataset. (F) E2F6 expression in patients with the indicated histologic grades and pathologic stages. (G) Expression of UPF3B mRNA was examined by quantitative RT-PCR (qRT-PCR) in control and E2F6-knocked down hepatocellular carcinoma (HCC) cells. (H) Protein levels of UPF3B were determined by western blotting in control and E2F6-knocked down HCC cells. (I) ChIP qRT-PCR analysis (left) shows that E2F6 binds to the UPF3B promoter in HepG2 cells. PCR products were subjected to agarose electrophoresis (right). (J) Western blot analysis of E2F6 and UPF3B protein levels in paired HCC samples (T) and normal tissues (N). **p* < 0.05, ***p* < 0.01, ****p* < 0.001. TPM, transcripts per million.



after overexpression of *UPF3B* in SNU-387, Hep3B, and HuH-7 cells (Figure 4C). Both RIP and qRT-PCR confirmed the binding of *UPF3B* protein to *PPP2R2C* mRNA in MHCC97H cells, while *UPF3B* interference attenuated this interaction (Figure 4D). Analysis of mRNA stability showed that the knockdown of *UPF3B* restrained the

mRNA decay of *PPP2R2C* in HepG2 and MHCC97H cells (Figure 4E). Next, qRT-PCR confirmed the efficiency of *PPP2R2C* interference (Figure 4F). The knockdown of *PPP2R2C* abolished the suppression of cell proliferation and p-AKT and p-S6 levels by *UPF3B* interfering in HepG2 and MHCC97H cells (Figure 4G,H). The above findings

indicate that UPF3B binds to *PPP2R2C* to accelerate its mRNA degradation, activating the PI3K/AKT/mTOR signaling.

3.5 | E2F6 induces UPF3B transcription

To delve deeper into the molecular mechanisms underlying the aberrant expression of UPF3B in HCC, an exploration of upstream mechanisms was carried out, involving the analysis of CNV, DNA methylation, N6-methyladenosine (m6A) methylation, and transcription factors. As shown in Figure S3A, analysis of the online database MEXPRESS indicated that the expression level of *UPF3B* was independent of gene CNV and only weakly correlated with the DNA methylation status of the promoter. After treatment of HCC cells with decitabine, a DNA methyltransferase inhibitor, qRT-PCR findings indicated that the expression of *UPF3B* was not affected by DNA methylation in HepG2 or MHCC97H cells (Figure S3B). Similarly, no significant changes in UPF3B expression levels were observed after interfering with METTL3, METTL14, or METTL3/14 inhibitor (Figure S3C,D).

Subsequently, transcription factors related to *UPF3B* promoter were screened from the hTFtarget database, and the genes correlated with *UPF3B* expression ($r > 0.3$) were screened from the cBioPortal database. The intersection of the above results obtained 10 potential transcription factors: CFBF, LMNB1, BRCA1, TFDP1, TAF1, CREB1, SUZ12, E2F6, E2F7, E2F3 (Figure 5A). The GSE14520 dataset was used to verify their correlation with UPF3B expression ($r > 0.3$), narrowing the number of potential transcription factors to five (Figure S4A). Their binding reliability to *UPF3B* promoter was further validated by Cistrome Data Browser, in which the binding scores > 1 were BRCA1, E2F6, and SUZ12 (Table S3). Next, survival analysis of the above three transcription factors was undertaken in TCGA-LIHC and GSE14520 datasets. The findings indicated that individuals with elevated expression of *E2F6* and *BRCA1* had significantly shorter survival (Figures 5C,D and S4B,C). Furthermore, *E2F6* and *BRCA1* showed elevated expression in HCC samples compared with normal tissues (Figures 5E and S4D). Elevated *UPF3B* expression was also observed in patients with advanced histologic grades and pathologic stages (Figures 5F and S4E). After interfering with *E2F6* in HepG2 and MHCC97H cells, UPF3B mRNA and protein levels were significantly decreased (Figure 5G,H), while no marked variance in *UPF3B* expression levels was noted after interfering with *BRCA1* (Figure S4F). To ascertain whether *E2F6* directly regulates UPF3B transcription, binding sites of *E2F6* on the *UPF3B* promoter were predicted using the JASPAR database. The ChIP analysis in HepG2 cells further substantiated that *E2F6* binds to the *UPF3B* promoter

(Figure 5I), thereby exerting regulatory control over the expression of *UPF3B*. Western blot analysis on clinical specimens collected from HCC patients verified that *E2F6* and UPF3B were highly expressed in HCC samples compared with matched normal tissues (Figure 5J).

3.6 | E2F6/UPF3B axis promoted HCC growth through PI3K/AKT/mTOR pathway

It has been reported that *E2F6* is a member of the E2F family that could control cell proliferation.^{18–20} To elucidate whether *E2F6* functions on the proliferative capacity of HCC through UPF3B, qRT-PCR revealed that knocking down UPF3B after *E2F6* overexpression restored UPF3B expression in HepG2 and MHCC97H cells (Figure 6A). The CCK-8 assay (Figure 6B), EdU assay (Figure 6C), and colony formation assay (Figure 6D) showed that UPF3B interference reversed the *E2F6*-enhanced proliferation of these cells.

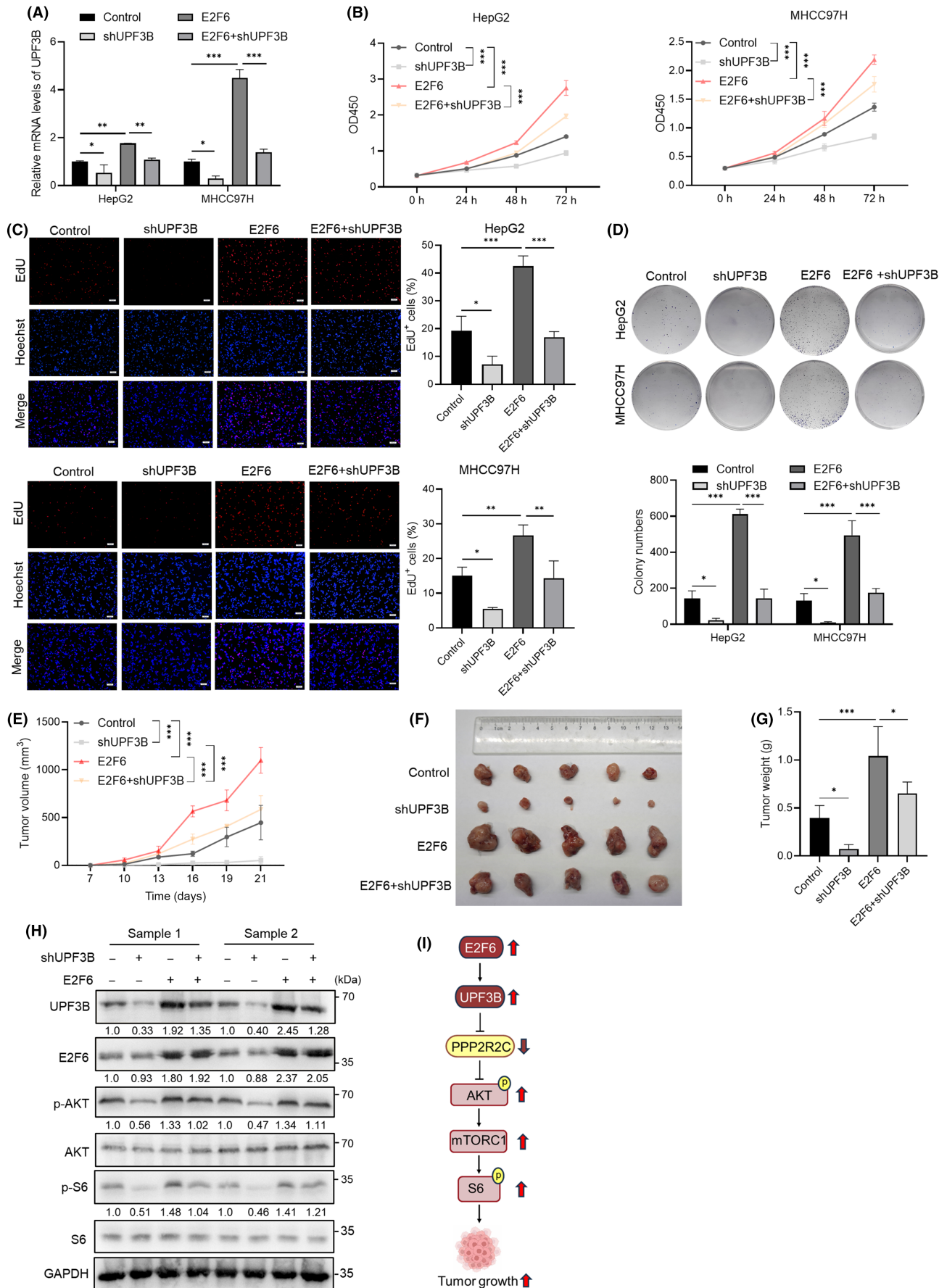
The role of the *E2F6/UPF3B* axis in tumor development was further explored using a mouse xenograft model. As shown in Figure 6E–G, interference with UPF3B in MHCC97H cells was able to reverse the elevated tumor volume and weight induced by overexpression of *E2F6*. Western blot analysis of the xenografts showed that the levels of p-AKT and p-S6 were considerably enhanced after *E2F6* overexpression but decreased after interference with UPF3B (Figure 6H). In summary, the *E2F6/UPF3B* axis regulated the PI3K/AKT/mTOR signaling to promote HCC growth.

4 | DISCUSSION

High transcriptional levels of *UPF3B* were associated with worse prognosis in multiple cancer types,²¹ although the molecular mechanisms of UPF3B in tumor progression are unclear. As an RBP, UPF3B can directly bind to the target mRNA and induce mRNA degradation.^{11,12} This study identified an *E2F6/UPF3B/PPP2R2C* axis that drives HCC growth (Figure 6I). First, UPF3B expression was notably elevated in HCC tissues relative to normal liver tissues and associated with poor patient prognosis. Second, overexpression of UPF3B enhanced the proliferative capacity of HCC cells. Additionally, elevated expression of UPF3B was driven by the upregulation of *E2F6* in HCC tissues and UPF3B-bound *PPP2R2C*, accelerating its RNA degradation and mediating the activation of the PI3K/AKT/mTOR signaling.

E2F is a family of transcription factors critically regulating eukaryotic cell proliferation. In mammals, eight members of the E2F family (*E2F1–E2F8*) have been identified.^{22,23} *E2F6* performs its biological

FIGURE 6 *E2F6/UPF3B* axis promotes hepatocellular carcinoma (HCC) growth and the activation of PI3K/AKT/mTOR signaling. (A) Expression of *UPF3B* was examined by quantitative RT-PCR in HCC cells with *E2F6* overexpression and *UPF3B* interference. (B) CCK-8, (C) EdU, and (D) colony-formation assays in HCC cells with *E2F6* overexpression and *UPF3B* interference. (E) Subcutaneous xenograft volume was measured every 3 days. (F) Images and (G) weight of tumors collected at 21 days postinoculation ($n = 5$). (H) Western blot analysis of proteins associated with the PI3K/AKT/mTOR signaling in the xenograft tumors. (I) Proposed model for the role of the *E2F6/UPF3B/PPP2R2C* axis in promoting HCC growth through the PI3K/AKT/mTOR signaling. * $p < 0.05$, ** $p < 0.01$, *** $p < 0.001$. OD450, optical density at 450 nm.



role by altering the transcription of downstream genes through binding to the DNA site 5'-TCCGC-3'.²⁴ Extensive research has highlighted the elevated expression of E2F6 in diverse cancers, facilitating the growth of tumor cells.²⁵ By binding to the *PNO1* promoter, E2F6 upregulates *PNO1* expression and enhances the progression of triple-negative breast cancer.²⁶ However, the mechanism of action between UPF3B and E2F6 remains unexplored. This research determined that E2F6 showed elevated expression in HCC tissues and was linked with adverse prognosis. Binding to the *UPF3B* promoter, E2F6 upregulated the expression of UPF3B, subsequently promoting the growth of HCC. It is worth noting that when UPF3B was knocked down after E2F6 overexpression, the cell growth was slightly higher than that of the control group (Figure 6B), suggesting that UPF3B might not be the sole target of E2F6 in promoting cell proliferation.

The PI3K/AKT/mTOR signaling could regulate apoptosis, cell cycle, metabolism, and angiogenesis, offering a wide range of therapeutic possibilities.²⁷ The AKT signaling could be dephosphorylated by PP2A.²⁸ We found that *PPP2R2C*, a regulatory subunit of PP2A, is the target of UPF3B. *PPP2R2C* has been proven to be a tumor suppressor.²⁹ *PPP2R2C* is downregulated in glioma tissues and cells and inhibits the mTOR pathway, thus inhibiting tumor growth.³⁰ It has also been reported that the expression of *PPP2R2C* is downregulated in primary prostate cancer, and its low expression is related to poor survival and prognosis of patients.³¹ Our results are consistent with this: UPF3B can bind to *PPP2R2C*, accelerate its mRNA degradation, and then activate the PI3K/AKT/mTOR signal transduction pathway to promote the proliferation of HCC cells. Similarly, a recent study showed that UPF3B-S (a truncated oncogenic splice variant) drives metastasis in HCC by targeting the 3'-UTR of *CDH1* mRNA to enhance its degradation.³² However, the particular sites of *PPP2R2C* mRNA that bind to UPF3B protein require further examination.

In conclusion, this research indicates that UPF3B predicts an unfavorable prognosis in individuals with HCC. In addition, this study reveals that the E2F6/UPF3B/*PPP2R2C* axis mediates the activation of PI3K/AKT/mTOR signaling to promote HCC growth. Therefore, targeting the E2F6/UPF3B/*PPP2R2C* axis could be a promising strategy for treating HCC.

AUTHOR CONTRIBUTIONS

Bowen Hou: Data curation; formal analysis; investigation; methodology; visualization; writing – original draft. **Min Shu:** Data curation; formal analysis; investigation; methodology; validation; visualization; writing – original draft. **Chenghao Liu:** Conceptualization; data curation; methodology; software. **Yunfeng Du:** Data curation; methodology; resources; software. **Cuicui Xu:** Data curation; methodology; resources. **Huijiao Jiang:** Data curation; methodology; resources. **Jun Hou:** Data curation; methodology; supervision; writing – review and editing. **Xueling Chen:** Data curation; methodology; supervision; writing – review and editing. **Lianghai Wang:** Conceptualization; funding acquisition; supervision; writing – review and editing. **Xiangwei Wu:** Conceptualization; funding acquisition; methodology; supervision; writing – review and editing.

ACKNOWLEDGMENTS

None.

FUNDING INFORMATION

This work was supported by the National Natural Science Foundation of China (82360503), the Bingtuan Science and Technology Program (2021BC002), Tianshan Talents – Science and Technology Innovation Team Project (2023TSYCTD0020), and the Non-profit Central Research Institute Fund of Chinese Academy of Medical Sciences (2020-PT330-003).

CONFLICT OF INTEREST STATEMENT

The authors declare no conflict of interest.

DATA AVAILABILITY STATEMENT

The original contributions presented in the study are included in the article/supplementary material. Further inquiries can be directed to the corresponding authors.

ETHICS STATEMENTS

Approval of the research protocol by an Institutional Review Board: The study was approved by the Biology Ethics Committee of Shihezi University and the Science and Technology Ethical Committee of the First Affiliated Hospital of Shihezi University.

Informed consent: N/A.

Registry and the Registration No. of the study/trial: N/A.

Animal studies: The experimental protocols utilized in this research were approved by the Biology Ethics Committee of Shihezi University.

ORCID

Min Shu  <https://orcid.org/0009-0006-6983-6836>

Chenghao Liu  <https://orcid.org/0000-0002-5432-3118>

Lianghai Wang  <https://orcid.org/0000-0003-3128-7780>

REFERENCES

- Bray F, Laversanne M, Sung H, et al. Global cancer statistics 2022: GLOBOCAN estimates of incidence and mortality worldwide for 36 cancers in 185 countries. *CA Cancer J Clin.* 2024;74:229-263.
- Forrester SJ, Dolmatova EV, Griendling KK. An acceleration in hypertension-related mortality for middle-aged and older Americans, 1999-2016: an observational study. *PLoS One.* 2020;15:e0225207.
- Lu LC, Hsu CH, Hsu C, Cheng AL. Tumor heterogeneity in hepatocellular carcinoma: facing the challenges. *Liver Cancer.* 2016;5:128-138.
- Llovet JM, Kelley RK, Villanueva A, et al. Hepatocellular carcinoma. *Nat Rev Dis Primers.* 2021;7:6.
- Yang JD, Hainaut P, Gores GJ, Amadou A, Plymoth A, Roberts LR. A global view of hepatocellular carcinoma: trends, risk, prevention and management. *Nat Rev Gastroenterol Hepatol.* 2019;16:589-604.
- Gebauer F, Preiss T, Hentze MW. From cis-regulatory elements to complex RNPs and back. *Cold Spring Harb Perspect Biol.* 2012;4:a012245.
- Hentze MW, Castello A, Schwarzl T, Preiss T. A brave new world of RNA-binding proteins. *Nat Rev Mol Cell Biol.* 2018;19:327-341.

8. Neelamraju Y, Hashemikhabir S, Janga SC. The human RBPome: from genes and proteins to human disease. *J Proteome*. 2015;127:61-70.
9. Kechavarzi B, Janga SC. Dissecting the expression landscape of RNA-binding proteins in human cancers. *Genome Biol*. 2014;15:R14.
10. Wang ZL, Li B, Luo YX, et al. Comprehensive genomic characterization of RNA-binding proteins across human cancers. *Cell Rep*. 2018;22:286-298.
11. Gao Z, Wilkinson M. An RNA decay factor wears a new coat: UPF3B modulates translation termination. *F1000Res*. 2017;6:2159.
12. Tan K, Jones SH, Lake BB, et al. The role of the NMD factor UPF3B in olfactory sensory neurons. *elife*. 2020;9:e57525.
13. Pozdeyev N, Gay LM, Sokol ES, et al. Genetic analysis of 779 advanced differentiated and anaplastic thyroid cancers. *Clin Cancer Res*. 2018;24:3059-3068.
14. Zhongxia Y, René MA, Sean M, et al. Mammalian UPF3A and UPF3B can activate nonsense-mediated mRNA decay independently of their exon junction complex binding. *EMBO J*. 2022;41:e109202.
15. Zhu W, Zhang Q, Liu M, Yan M, Chu X, Li Y. Identification of DNA repair-related genes predicting pathogenesis and prognosis for liver cancer. *Cancer Cell Int*. 2021;21:81.
16. Wang L, Li X, Zhao L, et al. Identification of DNA-repair-related five-gene signature to predict prognosis in patients with esophageal cancer. *Pathol Oncol Res*. 2021;27:596899.
17. Jäger K, Mensch J, Grimmig ME, et al. A conserved long-distance telomeric silencing mechanism suppresses mTOR signaling in aging human fibroblasts. *Sci Adv*. 2022;8:eabk2814.
18. Giangrande PH, Zhu W, Schlisio S, et al. A role for E2F6 in distinguishing G1/S- and G2/M-specific transcription. *Genes Dev*. 2004;18:2941-2951.
19. Gaubatz S, Wood JG, Livingston DM. Unusual proliferation arrest and transcriptional control properties of a newly discovered E2F family member, E2F-6. *Proc Natl Acad Sci USA*. 1998;95:9190-9195.
20. Pennycook BR, Vesela E, Peripolli S, et al. E2F-dependent transcription determines replication capacity and S phase length. *Nat Commun*. 2020;11:3503.
21. Xu J, Ma H, Shan B. Up-frameshift suppressor 3 as a prognostic biomarker and correlated with immune infiltrates: a pan-cancer analysis. *PLoS One*. 2022;17:e0273163.
22. Lambert SA, Jolma A, Campitelli LF, et al. The human transcription factors. *Cell*. 2018;175:598-599.
23. Chen HZ, Tsai SY, Leone G. Emerging roles of E2Fs in cancer: an exit from cell cycle control. *Nat Rev Cancer*. 2009;9:785-797.
24. Kehoe SM, Oka M, Hankowski KE, et al. A conserved E2F6-binding element in murine meiosis-specific gene promoters. *Biol Reprod*. 2008;79:921-930.
25. Trimarchi JM, Lees JA. Sibling rivalry in the E2F family. *Nat Rev Mol Cell Biol*. 2002;3:11-20.
26. Shao G, Fan X, Zhang P, Liu X, Huang L, Ji S. Circ_0004676 exacerbates triple-negative breast cancer progression through regulation of the miR-377-3p/E2F6/PNO1 axis. *Cell Biol Toxicol*. 2023;39:2183-2205.
27. Manning BD, Toker A. AKT/PKB signaling: navigating the network. *Cell*. 2017;169:381-405.
28. Nitulescu GM, Van De Venter M, Nitulescu G, et al. The Akt pathway in oncology therapy and beyond (review). *Int J Oncol*. 2018;53:2319-2331.
29. Hu P, Yu L, Zhang M, et al. Molecular cloning and mapping of the brain-abundant B1gamma subunit of protein phosphatase 2A, PPP2R2C, to human chromosome 4p16. *Genomics*. 2000;67:83-86.
30. Fan YL, Chen L, Wang J, Yao Q, Wan JQ. Over expression of PPP2R2C inhibits human glioma cells growth through the suppression of mTOR pathway. *FEBS Lett*. 2013;587:3892-3897.
31. Bluemn EG, Spencer ES, Mecham B, et al. PPP2R2C loss promotes castration-resistance and is associated with increased prostate cancer-specific mortality. *Mol Cancer Res*. 2013;11:568-578.
32. Wang H, Qian D, Wang J, et al. HnRNPR-mediated UPF3B mRNA splicing drives hepatocellular carcinoma metastasis. *J Adv Res*. 2024.

SUPPORTING INFORMATION

Additional supporting information can be found online in the Supporting Information section at the end of this article.

How to cite this article: Hou B, Shu M, Liu C, et al. Unveiling the role of UPF3B in hepatocellular carcinoma: Potential therapeutic target. *Cancer Sci*. 2024;115:2646-2658. doi:[10.1111/cas.16240](https://doi.org/10.1111/cas.16240)